IIETA International Information and Engineering Technology Association
Advancing the World of Information and Engineering

Revue des Composites et des Matériaux Avancés-Journal of Composite and Advanced Materials
Vol. 36, No. 1, February, 2026, pp. 97-106
Journal homepage: http://iieta.org/journals/rcma

Thermally Induced Vibration Behavior of Laminated Composite Plates: A Four-Variable Refined Plate Theory Approach

Ahmed K. Sabea*, Widad I. Majeed

Mechanical Department, College of Engineering, University of Baghdad, Baghdad 10071, Iraq

Corresponding Author Email: Ahmed.Sabie2503m@coeng.uobaghdad.edu.iq

Copyright: ©2026 The authors. This article is published by IIETA and is licensed under the CC BY 4.0 license (http://creativecommons.org/licenses/by/4.0/).

https://doi.org/10.18280/rcma.360110

Received: 13 December 2025
Revised: 2 February 2026
Accepted: 15 February 2026
Available online: 28 February 2026

Keywords:
natural frequency, thermal loads, laminated plates, refined plate theory, four variables, shear deformation theory

ABSTRACT

The present work proposes a four-variable refined theory for modelling free vibration of composite plates under thermal loading. The shape function comprises hyperbolic and polynomial terms for the first time to investigate natural frequencies in the thermal environment of cross- and angle-laminated plates. The dynamic governing equations are derived via variational framework of Hamilton's principle by the transverse shear stress field follows a parabolic function through the plate's depth, which yields zero traction on the free plate surfaces. A closed-form solution is conducted based on Navier's solution with simply supported boundary conditions. The embedded shape function which was used for the first time in the free vibration under thermal loads analysis within proposed theory successfully provided less computational complexity yet convergence accuracy in predicting composite plates dynamic behavior in thermal environment compared to high order theory which involved computational challenges. Transverse shear stresses are directly modeled in the present theory, without requiring shear correction factor. The proposed theory results are consistent with other theories from the literature for both studied plates (thick and thin). Also, the influence of a range of design factors, including layer schemes, orthotropic modulus ratio, and thickness ratio, on the fundamental frequency of laminated composite plates under thermal loads have been analyzed.

1. INTRODUCTION

Laminate composite plates are extensively employed in modern aerospace industries, especially drones, due to their high stiffness-to-weight ratio. However, in service, temperature fluctuations can induce thermal stresses that adversely affect structural behavior, particularly by lowering natural frequencies and increasing the likelihood of vibration. Elevating the priority of researching the area of free vibration in thermal environments, such studies provide an insight into the thermo-mechanical coupling effect (vibration behavior of materials at high temperature, which differs from its behavior at room temperature), structural stability and safety, reliability, fatigue resistance, and advanced theories validation. Classical plate theory, one of the earlier theories proposed to assess laminated plates, loses its validity for multilayer composites by ignoring the critical influence of transverse shear.

Jameel and Hussien [1] investigated vibration of laminated plates influenced by thermal and mechanical or free vibration to show the effect of design variables such as geometric ratios, boundary conditions, and ply orientation angle based on classical plate theory. The study included analytical, numerical, and experimental analysis to demonstrate and confirm the effect of design parameters and the impact of thermal conditions on both natural and forced vibration. Majeed and Tayeh [2] also adopted classical plate theory to analyze the buckling stability and natural vibration characteristics of composite plates under in-plane compressive forces. Hamilton's principle serves as the basis for establishing the governing equations, and a closed-form solution was obtained based on the Ritz method to exhibit the influence of design parameters on plate buckling and vibration. Hammed and Majeed [3] analysed free vibration of laminated thin plates resting on an elastic foundation based on classical plate theory. By applying the Ritz method and the imaginary spring technique, results were obtained, and researchers examined the effects of parameters such as (layers scheme, aspect ratio, thickness ratio, and the ratio of initial in-plane thermal load). According to the study, the influence of aspect ratio on natural frequency was between 35% and 40%. First-order shear deformation theory was proposed to overcome the physically inaccurate and overly restrictive kinematics assumption of the classical plate theory, but the theory fails to account for zero transverse shear stress on free surfaces of the plate, demanding a shear correction factor to overcome its miscalculations. Patro et al. [4] investigated the natural frequency of stiffened composite plates when subjected to thermal stresses via a finite element approach that incorporates first-order shear deformation theory in the ANSYS framework, providing numerical data that demonstrated the effect of (temperature, modulus ratio, and coefficient of thermal expansion). The results indicated that elevated temperature decreases natural

frequency values. Results of the Das and Niyogi [5] study showed that increased structural stiffness correlates with an enhanced ability to withstand the combined effects of high temperature and moisture content. Wu et al. [6] used a numerical approach that combines the quadrature method with an iterative procedure, derived from Hamilton's principle using a first-order shear deformation theory that accounts for von Karaman type geometric nonlinearity, to analyze large-amplitude vibrations Graphene-Platelet-Reinforced nanocomposite multilayer annular plates in a thermal environment. Employing a layer-based computational model, Zhai et al. [7] explored how composite sandwich plates vibrate and buckle when exposed to heat. The formulation, suitable for a range of plate thicknesses, incorporates thermal effects on material displacements. Other studies on the dynamic response of functionally graded nanoplates under free vibration were presented, considering two structural configurations. The model incorporates small-scale effects via the nonlocal elasticity theory of Eringen and uses a higher-order formulation to derive governing equations for simply supported plates, accounting for temperature-dependent material properties [8]. Ibrahim and Ghani [9] use the Rayleigh-Ritz approach to investigate the free vibration of a composite plate having general elastic fixing along its edges. By introducing sinusoidal and arbitrary continuous functional components as shape functions, the study's numerical results showed good agreement with the literature. A study conducted by Hellal et al. [10] proposed a four-unknown shear deformation theory to investigate dynamic and buckling effects by hygro-thermal ambiance, using a functionally graded sandwich plate model supported by Winkler Pasternak elastic foundations. They added an integral term to the displacement field, thereby reducing the number of variables and the number of basic equations. Kallannavar et al. [11] used first-order deformation theory to examine the impact of temperature and moisture on bias lamination of a composite sandwich plate. The novelty of the work lies in the use of the artificial neural network technique; the model uses graphite-epoxy composite laminates as the face sheet and DYAD 606 viscoelastic material as the core. Moradi-Dastjerdi and Behdinan [12] introduced a novel intelligent sandwich structure with a five-lamina structure, a porous core, intermediate polymer/graphene nanocomposite layers, and outer piezoelectric faces. The investigation focuses on how temperature, piezoelectric effects, and an elastic foundation influence the plate's natural frequencies. A free vibration analysis under thermal loads was conducted by Yahea and Majeed [13] for laminates with [0/90] and [±θ] ply configurations, employing trigonometric four-variable theory, applying the Hamilton principle to derive the governing equations, and using the Navier solution to evaluate the system's undamped free-vibration frequencies, and compared to previous studies, showing good agreement. Draiche and Tounsi [14] proposed an innovative hyperbolic shear deformation theory for investigating the flexural and dynamic response of cross-ply laminated spherical shells. A refined plate theory proposed by Sadiq and Bawa [15] was used to model and evaluate the oscillatory motion of [0/90] laminated structure under initial stresses, with simply supported fixing, via Hamilton's principle alongside computational output acquired from Navier's solution, and validate against published findings. The work of Sahu et al. [16] investigates the vibration and dynamic transient response of hybrid laminated composite panels using a finite element model and compares it with in-house experimental data. The modal influence due to thermal loading was calculated using a higher-order displacement polynomial. Saini and Lal [17] applied first-order deformation theory to analyze the vibration of a bi-directional functionally graded circular plate under a two-dimensional thermal load, based on the energy-based Hamilton principle. The governing equations were derived; furthermore, numerical results were evaluated using the differential quadrature method. The study of Azzara et al. [18] focuses on vibration and buckling analysis of composite structures in a thermal environment using the Carrara unified formulation, employing Lagrange-like polynomials to define the motion and deformation, as well as layer-wise theories to describe the complex behavior within the composite structure. The study of Udaiwal and Sharma [19] develops a comprehensive finite element methodology to analyze the dynamic stability of layered composite and sandwich plates and beams influenced by thermal loads. The research highlights the significant influence of ply-angle, revealing that a 45° orientation maximizes non-dimensional frequency, independent of geometric ratios. Guo et al. [20] investigate the control of nonlinear and thermally coupled vibrations in flexible spacecraft solar panels. Using a finite element model of a panel with active constrained-layer damping, the research analyzes how piezoelectric patch placement, coverage, rotational speed, and damping-layer thickness affect vibration suppression. Using a strong-form collocation method using only nodal points, Kwak et al. [21] analyzed the vibration and dynamic response of laminated composite wave plates. Researchers proposed a first-order theory and derived the governing equation based on the Hamilton principle. A meshfree interpolation function that blends Tchebychev polynomials with radial basis functions, with a point interpolation framework, approximates the displacement components. Majeed and Sadiq [22] proposed, for the first time, a combination of hyperbolic and polynomial four-variable refined theory for buckling analysis of rectangular composite plates, achieving zero traction on the free transverse surfaces of a simply supported model plate. Based on the virtual displacement principle and Navier's method, the equation of motion was derived, as well as a closed form established. Numerical results show good agreement compared to other studies. While the literature included numerous studies on the free vibration of composite plates in thermal environments, this field continues to evolve. Consequently, further research utilizing diverse theories and shape functions is required to expand the repertoire of analytical modeling approaches for diverse application needs.

To this end, the present study investigates the free vibration of laminated composite plates under thermal load using the four-variable shear deformation theory. Zero transverse shear stresses on the upper and lower surfaces are achieved by a combination of hyperbolic and polynomial shape functions proposed by the study [14]. Using the virtual displacement principle to determine the governing equations, as well as the Navier solution method of simply supported fixing, to produce a closed-form solution. The results of this study are benchmarked against previous studies and show good agreement. The analysis also examines the effect of critical design factors, including stacking sequence, orthotropic modulus ratio, and thickness ratio, on the fundamental frequency of composite plates in a thermal environment.

2. THEORY AND FORMULATION

The problem considers a laminated composite plate in a thermal environment, with plate dimensions (a,b).

2.1 Kinematics

The formulation of the displacement field is grounded [23] as:

$$u_{(x,y,z)} = u_{0(x,y)} + z\left(-\frac{\partial w^b}{\partial x}\right) + F(z)\left(-\frac{\partial w^s}{\partial x}\right) \tag{1}$$

$$v_{(x,y,z)} = v_{0(x,y)} + z\left(-\frac{\partial w^b}{\partial y}\right) + F(z)\left(-\frac{\partial w^s}{\partial y}\right) \tag{2}$$

$$w_{(x,y,z)} = w^b_{(x,y)} + w^s_{(x,y)} \tag{3}$$

where, u_o, v_o, w^b and w^s are the four components of displacement, $F(z)$ represents the shape function of the theorem, which describes the through-thickness profile of transverse shear stress, achieving zero stress at the free edges of the plate. For the present study, it was defined according to Draiche and Tounsi [14] as:

$$F(z) = z - h\left(\sinh\left(\frac{z}{h}\right)\right) + \left(\left(\frac{4z^3}{3h^2}\right)\cosh(0.5)\right) \tag{4}$$

2.2 Strain relations

Following Reddy [24]. The equations that relate strain to displacement linearly are written as:

$$\varepsilon_{ij} = \frac{1}{2}\left(U_{i,j} + U_{j,i}\right) \tag{5}$$

$$\begin{Bmatrix}\varepsilon_{xx}\\ \varepsilon_{yy}\\ \gamma_{xy}\end{Bmatrix} = \begin{Bmatrix}\varepsilon^0_{xx}\\ \varepsilon^0_{yy}\\ \gamma^0_{xy}\end{Bmatrix} + z\begin{Bmatrix}\varepsilon^1_{xx}\\ \varepsilon^1_{yy}\\ \gamma^1_{xy}\end{Bmatrix} + F(z)\begin{Bmatrix}\varepsilon^2_{xx}\\ \varepsilon^2_{yy}\\ \gamma^2_{xy}\end{Bmatrix} \tag{6}$$

$$\begin{Bmatrix}\gamma_{yz}\\ \gamma_{xz}\end{Bmatrix} = \begin{Bmatrix}\gamma^0_{yz}\\ \gamma^0_{xz}\end{Bmatrix} + F'(z)\begin{Bmatrix}\gamma^3_{yz}\\ \gamma^3_{xz}\end{Bmatrix} \tag{7}$$

$$\begin{Bmatrix}\gamma_{yz}\\ \gamma_{xz}\end{Bmatrix} = g(z)\begin{Bmatrix}\dfrac{\partial w^s}{\partial y}\\ \dfrac{\partial w^s}{\partial x}\end{Bmatrix} \tag{8}$$

$$g(z) = 1 - F'(z) = \cosh\left(\frac{z}{h}\right) + \left(\frac{4z^2}{h^2}\right)\cosh(0.5) \tag{9}$$

$$\varepsilon_{zz} = 0 \tag{10}$$

2.3 Equation of motion

The governing equations are derived using the Hamilton principle [24]:

$$0 = \int_0^T (\delta U + \delta V - \delta K)dt \tag{11}$$

where, δU: the virtual work of internal strains. δV: thermally induced virtual external work. δK: virtual kinetic energy.

$$\delta U = \int_{\Omega_0}^{K}\int_{z_k}^{z_{k+1}}\left[\begin{Bmatrix}\sigma_{xx}\\ \sigma_{yy}\\ \sigma_{xy}\end{Bmatrix}\begin{Bmatrix}\delta\varepsilon_{xx}\\ \delta\varepsilon_{yy}\\ \delta\gamma_{xy}\end{Bmatrix}^k + \begin{Bmatrix}\sigma_{yz}\\ \sigma_{xz}\end{Bmatrix}\begin{Bmatrix}\delta\gamma_{yz}\\ \delta\gamma_{xz}\end{Bmatrix}^k\right]dzdxdy \tag{12}$$

$$\delta U = \int_{\Omega_0}^{K}\left[\begin{Bmatrix}N_{xx}\\ N_{yy}\\ N_{xy}\end{Bmatrix}\begin{Bmatrix}\delta\varepsilon^0_{xx}\\ \delta\varepsilon^0_{yy}\\ \delta\gamma^0_{xy}\end{Bmatrix}^k + \begin{Bmatrix}M^b_{xx}\\ M^b_{yy}\\ M^b_{xy}\end{Bmatrix}\begin{Bmatrix}\delta\varepsilon^1_{xx}\\ \delta\varepsilon^1_{yy}\\ \delta\gamma^1_{xy}\end{Bmatrix} + \begin{Bmatrix}M^s_{xx}\\ M^s_{yy}\\ M^s_{xy}\end{Bmatrix}\begin{Bmatrix}\delta\varepsilon^2_{xx}\\ \delta\varepsilon^2_{yy}\\ \delta\gamma^2_{xy}\end{Bmatrix}^k + \begin{Bmatrix}Q_y\\ Q_x\end{Bmatrix}\begin{Bmatrix}\delta\gamma^0_{yz}\\ \delta\gamma^0_{xz}\end{Bmatrix}^k\right]dxdyy \tag{13}$$

$$\delta U = \int_{\Omega}^{k}\left[\begin{Bmatrix}N_{xx}\\ N_{yy}\\ N_{xy}\end{Bmatrix}\begin{Bmatrix}\dfrac{\partial\delta u_0}{\partial x}\\ \dfrac{\partial\delta v_0}{\partial y}\\ \dfrac{\partial\delta u_0}{\partial y} + \dfrac{\partial\delta v_0}{\partial x}\end{Bmatrix}^k - \begin{Bmatrix}M^b_{xx}\\ M^b_{yy}\\ M^b_{xy}\end{Bmatrix}\begin{Bmatrix}\dfrac{\partial^2\delta w^b}{\partial x^2}\\ \dfrac{\partial^2\delta w^b}{\partial y^2}\\ 2\dfrac{\partial^2 w^b}{\partial x\partial y}\end{Bmatrix}^k - \begin{Bmatrix}\dfrac{\partial^2\delta w^s}{\partial x^2}\\ \dfrac{\partial^2\delta w^s}{\partial y^2}\\ 2\dfrac{\partial^2\delta w^s}{\partial x\partial y}\end{Bmatrix}^k + \begin{Bmatrix}Q_y\\ Q_x\end{Bmatrix}\begin{Bmatrix}\dfrac{\partial\delta w^s}{\partial y}\\ \dfrac{\partial\delta w^s}{\partial x}\end{Bmatrix}^k\right]dxdy \tag{14}$$

$$\left(N_i, M^b_i, M^s_i\right) = \sum_{k=1}^{N}\int_{z_k}^{z_{k+1}}\sigma^k_i(1, z, F(z))dz, i = (xx, yy, xy) \tag{15}$$

$$\left(Q_j\right) = \sum_{k=1}^{N}\int_{z_k}^{z_{k+1}}\sigma^k_{jz}g(z)dz,\ j = (y, x) \tag{16}$$

$$\delta V = -\frac{1}{2}\int_{\Omega_0}^{K}\left[\begin{Bmatrix}N^T_{xx}\\ N^T_{yy}\\ N^T_{xy}\end{Bmatrix}\delta\begin{Bmatrix}\left(\dfrac{\partial w}{\partial x}\right)^2\\ \left(\dfrac{\partial w}{\partial y}\right)^2\\ \left(\dfrac{\partial w}{\partial x}\dfrac{\partial w}{\partial y}\right)\end{Bmatrix}^k\right]dxdy \tag{17}$$

$$\delta V = -\frac{1}{2}\int_{\Omega_0}^{K}\begin{matrix}N^T_{xx}\\ N^T_{yy}\\ N^T_{xy}\\ N^T_{xy}\end{matrix}\left[\begin{pmatrix}2\left(\dfrac{\partial w}{\partial x}\right)\left(\dfrac{\partial\delta w}{\partial x}\right)\\ 2\left(\dfrac{\partial w}{\partial y}\right)\left(\dfrac{\partial\delta w}{\partial y}\right)\\ \left(\dfrac{\partial\delta w}{\partial x}\dfrac{\partial w}{\partial y}\right)\\ \left(\dfrac{\partial w}{\partial x}\dfrac{\partial\delta w}{\partial y}\right)\end{pmatrix}^k\right]dxdy \tag{18}$$

where, the total deflection (w) is assumed to be the superposition of the deflections caused by bending (w^b) and shear (w^s) modes through the plate's thickness [23].

$$\begin{Bmatrix} N_{xx}^{\mathrm{T}} \\ N_{yy}^{\mathrm{T}} \\ N_{xy}^{\mathrm{T}} \end{Bmatrix} = \sum_{k=1}^{N} \int_{Z_k}^{Z_{k+1}} \begin{bmatrix} \bar{Q}_{11} & \bar{Q}_{12} & \bar{Q}_{16} \\ \bar{Q}_{12} & \bar{Q}_{22} & \bar{Q}_{26} \\ \bar{Q}_{16} & \bar{Q}_{26} & \bar{Q}_{66} \end{bmatrix} \begin{Bmatrix} \alpha_{xx} \\ \alpha_{yy} \\ 2\alpha_{xy} \end{Bmatrix} \Delta T_{cr} dz \tag{19}$$

$$\delta K = \int_{\Omega_0} \int_{Z_k}^{Z_{k+1}} \rho(\dot{u}\delta\dot{u} + \dot{v}\delta\dot{v} + \dot{w}\delta\dot{w}) dz dx dy \tag{20}$$

Substituting Eq. (14), Eq. (18) and Eq. (20) into Eq. (11) and integrating by parts to evaluate the equation of motion as:

$$\delta u_0 : \frac{\partial \mathrm{N}_{xx}}{\partial x} + \frac{\partial \mathrm{N}_{xy}}{\partial y} = \mathrm{I}_0 \left(\ddot{u}_0 \right) - \mathrm{I}_1 \left(\frac{\partial \ddot{w}^b}{\partial x} \right) - \mathrm{I}_3 \left(\frac{\partial \ddot{w}^s}{\partial x} \right) \tag{21}$$

$$\delta v_0 : \frac{\partial \mathrm{N}_{yy}}{\partial y} + \frac{\partial \mathrm{N}_{xy}}{\partial x} = \mathrm{I}_0 \left(\ddot{v}_0 \right) - \mathrm{I}_1 \left(\frac{\partial \ddot{w}^b}{\partial y} \right) - \mathrm{I}_3 \left(\frac{\partial \ddot{w}^s}{\partial y} \right) \tag{22}$$

$$\begin{aligned} \delta w^b : & \left(\frac{\partial^2 M_{xx}^b}{\partial x^2} + \frac{\partial^2 M_{yy}^b}{\partial y^2} + 2\frac{\partial^2 M_{xy}^b}{\partial x \partial y} \right) \\ & + \left(N_{xx}^T \frac{\partial^2 (w^b + w^s)}{\partial x^2} + N_{yy}^T \frac{\partial^2 (w^b + w^s)}{\partial y^2} \right. \\ & \left. + 2N_{xy}^T \frac{\partial^2 (w^b + w^s)}{\partial x \partial y} \right) \\ & = I_0 \left(\ddot{w}^b + \ddot{w}^s \right) + I_1 \left(\frac{\partial \ddot{u}_0}{\partial x} + \frac{\partial \ddot{v}_0}{\partial y} \right) \\ & - I_2 \left(\frac{\partial^2 \ddot{w}^b}{\partial x^2} + \frac{\partial^2 \ddot{w}^b}{\partial y^2} \right) \\ & - I_4 \left(\frac{\partial^2 \ddot{w}^s}{\partial x^2} + \frac{\partial^2 \ddot{w}^s}{\partial y^2} \right) \end{aligned} \tag{23}$$

$$\begin{aligned} \delta w^s : & \left(\frac{\partial^2 \mathrm{M}_{xx}^s}{\partial x^2} + \frac{\partial^2 \mathrm{M}_{yy}^s}{\partial y^2} + 2\frac{\partial^2 \mathrm{M}_{xy}^s}{\partial x \, \partial y} + \frac{\partial \mathrm{Q}_y}{\partial y} + \frac{\partial \mathrm{Q}_x}{\partial x} \right) \\ & + \left(\mathrm{N}_{xx}^{\mathrm{T}} \frac{\partial^2 (w^b + w^s)}{\partial x^2} + \mathrm{N}_{yy}^{\mathrm{T}} \frac{\partial^2 (w^b + w^s)}{\partial y^2} \right. \\ & \left. + 2\mathrm{N}_{xy}^{\mathrm{T}} \frac{\partial^2 (w^b + w^s)}{\partial x \, \partial y} \right) \\ & = \mathrm{I}_0 \left(\ddot{w}^b + \ddot{w}^s \right) + \mathrm{I}_3 \left(\frac{\partial \ddot{\mathrm{U}}_0}{\partial x} + \frac{\partial \ddot{w}_0}{\partial y} \right) \\ & - \mathrm{I}_4 \left(\frac{\partial^2 \ddot{w}^b}{\partial x^2} + \frac{\partial^2 \ddot{w}^b}{\partial y^2} \right) - \mathrm{I}_5 \left(\frac{\partial^2 \ddot{w}^b}{\partial x^2} + \frac{\partial^2 \ddot{w}^b}{\partial y^2} \right) \end{aligned} \tag{24}$$

$$\begin{aligned} I_m = \int_{z_k}^{z_{k+1}} \rho(1, z, z^2, zF(z), (F(z))^2) dz, m \\ = (1,2,3,4,5) \end{aligned} \tag{25}$$

The plane stress reduced stiffness (Q_{ij}) is:

$$\begin{aligned} \mathrm{Q}_{11} &= \frac{\mathrm{E}_1}{1 - \mathrm{v}_{12}\mathrm{v}_{21}} \\ \mathrm{Q}_{12} &= \frac{\mathrm{v}_{12}\mathrm{E}_2}{1 - \mathrm{v}_{12}\mathrm{v}_{21}} \\ \mathrm{Q}_{22} &= \frac{\mathrm{E}_2}{1 - \mathrm{v}_{12}\mathrm{v}_{21}} \end{aligned} \tag{26}$$

$$\begin{aligned} \mathrm{Q}_{44} &= \mathrm{G}_{23} \\ \mathrm{Q}_{55} &= \mathrm{G}_{13} \\ \mathrm{Q}_{66} &= \mathrm{G}_{12} \end{aligned} \tag{27}$$

The Stress-strain relations in (*x*,*y*,*z*) coordinates are:

$$\begin{Bmatrix} \sigma_{xx} \\ \sigma_{yy} \\ \sigma_{xy} \end{Bmatrix} = \begin{bmatrix} \bar{\mathrm{Q}}_{11} & \bar{\mathrm{Q}}_{12} & \bar{\mathrm{Q}}_{16} \\ \bar{\mathrm{Q}}_{12} & \bar{\mathrm{Q}}_{22} & \bar{\mathrm{Q}}_{26} \\ \bar{\mathrm{Q}}_{16} & \bar{\mathrm{Q}}_{26} & \bar{\mathrm{Q}}_{66} \end{bmatrix} \begin{Bmatrix} \varepsilon_{xx} \\ \varepsilon_{yy} \\ \gamma_{xy} \end{Bmatrix} \tag{28}$$

$$\begin{aligned} \begin{Bmatrix} N_{xx} \\ N_{yy} \\ N_{xy} \end{Bmatrix} &= \begin{bmatrix} \mathrm{A}_{11} & \mathrm{A}_{12} & \mathrm{A}_{16} \\ \mathrm{A}_{12} & \mathrm{A}_{22} & \mathrm{A}_{26} \\ \mathrm{A}_{16} & \mathrm{A}_{26} & \mathrm{A}_{66} \end{bmatrix} \begin{Bmatrix} \varepsilon_{xx}^0 \\ \varepsilon_{yy}^0 \\ \gamma_{xy}^0 \end{Bmatrix} \\ &+ \begin{bmatrix} \mathrm{B}_{11} & \mathrm{B}_{12} & \mathrm{B}_{16} \\ \mathrm{B}_{12} & \mathrm{B}_{22} & \mathrm{B}_{26} \\ \mathrm{B}_{16} & \mathrm{B}_{26} & \mathrm{B}_{66} \end{bmatrix} \begin{Bmatrix} \varepsilon_{xx}^1 \\ \varepsilon_{yy}^1 \\ \gamma_{xy}^1 \end{Bmatrix} \\ &+ \begin{bmatrix} \mathrm{E}_{11} & \mathrm{E}_{12} & \mathrm{E}_{16} \\ \mathrm{E}_{12} & \mathrm{E}_{22} & \mathrm{E}_{26} \\ \mathrm{E}_{16} & \mathrm{E}_{26} & \mathrm{E}_{66} \end{bmatrix} \begin{Bmatrix} \varepsilon_{xx}^2 \\ \varepsilon_{yy}^2 \\ \gamma_{xy}^2 \end{Bmatrix} \end{aligned} \tag{29}$$

$$\begin{aligned} \begin{Bmatrix} M_{xx}^b \\ M_{yy}^b \\ M_{xy}^b \end{Bmatrix} &= \begin{bmatrix} \mathrm{B}_{11} & \mathrm{B}_{12} & \mathrm{B}_{16} \\ \mathrm{B}_{12} & \mathrm{B}_{22} & \mathrm{B}_{26} \\ \mathrm{B}_{16} & \mathrm{B}_{26} & \mathrm{B}_{66} \end{bmatrix} \begin{Bmatrix} \varepsilon_{xx}^0 \\ \varepsilon_{yy}^0 \\ \gamma_{xy}^0 \end{Bmatrix} \\ &+ \begin{bmatrix} \mathrm{D}_{11} & \mathrm{D}_{12} & \mathrm{D}_{16} \\ \mathrm{D}_{12} & \mathrm{D}_{22} & \mathrm{D}_{26} \\ \mathrm{D}_{16} & \mathrm{D}_{26} & \mathrm{D}_{66} \end{bmatrix} \begin{Bmatrix} \varepsilon_{xx}^1 \\ \varepsilon_{yy}^1 \\ \gamma_{xy}^1 \end{Bmatrix} \\ &+ \begin{bmatrix} \mathrm{F}_{11} & \mathrm{F}_{12} & \mathrm{F}_{16} \\ \mathrm{F}_{12} & \mathrm{F}_{22} & \mathrm{F}_{26} \\ \mathrm{F}_{16} & \mathrm{F}_{26} & \mathrm{F}_{66} \end{bmatrix} \begin{Bmatrix} \varepsilon_{xx}^2 \\ \varepsilon_{yy}^2 \\ \gamma_{xy}^2 \end{Bmatrix} \end{aligned} \tag{30}$$

$$\begin{aligned} \begin{Bmatrix} M_{xx}^s \\ M_{yy}^s \\ M_{xy}^s \end{Bmatrix} &= \begin{bmatrix} \mathrm{E}_{11} & \mathrm{E}_{12} & \mathrm{E}_{16} \\ \mathrm{E}_{12} & \mathrm{E}_{22} & \mathrm{E}_{26} \\ \mathrm{E}_{16} & \mathrm{E}_{26} & \mathrm{E}_{66} \end{bmatrix} \begin{Bmatrix} \varepsilon_{xx}^0 \\ \varepsilon_{yy}^0 \\ \gamma_{xy}^0 \end{Bmatrix} \\ &+ \begin{bmatrix} \mathrm{F}_{11} & \mathrm{F}_{12} & \mathrm{F}_{16} \\ \mathrm{F}_{12} & \mathrm{F}_{22} & \mathrm{F}_{26} \\ \mathrm{F}_{16} & \mathrm{F}_{26} & \mathrm{F}_{66} \end{bmatrix} \begin{Bmatrix} \varepsilon_{xx}^1 \\ \varepsilon_{yy}^1 \\ \gamma_{xy}^1 \end{Bmatrix} \\ &+ \begin{bmatrix} \mathrm{H}_{11} & \mathrm{H}_{12} & \mathrm{H}_{16} \\ \mathrm{H}_{12} & \mathrm{H}_{22} & \mathrm{H}_{26} \\ \mathrm{H}_{16} & \mathrm{H}_{26} & \mathrm{H}_{66} \end{bmatrix} \begin{Bmatrix} \varepsilon_{xx}^2 \\ \varepsilon_{yy}^2 \\ \gamma_{xy}^2 \end{Bmatrix} \end{aligned} \tag{31}$$

$$\begin{Bmatrix} \mathrm{Q}_y \\ \mathrm{Q}_x \end{Bmatrix} = \begin{bmatrix} \mathrm{L}_{44} & \mathrm{L}_{45} \\ \mathrm{L}_{45} & \mathrm{L}_{55} \end{bmatrix} \begin{Bmatrix} \gamma_{yz}^0 \\ \gamma_{xz}^0 \end{Bmatrix} \tag{32}$$

$$\begin{Bmatrix} A_{ij} \\ B_{ij} \\ D_{ij} \\ E_{ij} \\ F_{ij} \\ H_{ij} \end{Bmatrix} = \int_{z_k}^{z_{k+1}} \bar{Q}_{ij} \begin{Bmatrix} 1 \\ z \\ z^2 \\ F(z) \\ zF(z) \\ (F(z))^2 \end{Bmatrix} dz, (i,j) = (1,2,6) \tag{33}$$

$$L_{ij} = \int_{z_k}^{z_{k+1}} Q_{\mathrm{ij}} (g(z))^2 dz, (i,j) = (4,5) \tag{34}$$

2.4 Navier solution

The analytical solution was derived using Navier's method, which required simply supported boundary conditions. Accordingly, distinct displacement expansions for cross-ply

and angle-ply laminates were adopted from [23]:

$$\text{at } x = 0 \text{ and } x = a: v_0 = w^b = w^s = M_x^b = M_x^s = 0 \quad (35)$$

$$\text{at } y = 0 \text{ and } y = b: u_0 = w^b = w^s = M_y^b = M_y^s = 0 \quad (36)$$

$$u_{0(x,y,t)} = \sum_{n=1}^{\infty}\sum_{m=1}^{\infty} U_{mn}\cos\ \alpha x \sin\ \beta y \quad (37)$$

$$v_{0(x,y,t)} = \sum_{n=1}^{\infty}\sum_{m=1}^{\infty} V_{mn}\sin\ \alpha x \cos\ \beta y \quad (38)$$

$$w^b_{(x,y,t)} = \sum_{n=1}^{\infty}\sum_{m=1}^{\infty} W^b_{mn}\sin\ \alpha x \sin\ \beta y \quad (39)$$

$$w^s_{(x,y,t)} = \sum_{n=1}^{\infty}\sum_{m=1}^{\infty} W^s_{mn}\sin\ \alpha x \sin\ \beta y \quad (40)$$

$$\text{at } x = 0 \text{ and } x = a: v_0 = w^b = w^s = M_x^b = M_x^s = 0 \quad (41)$$

$$\text{at } y = 0 \text{ and } y = b: u_0 = w^b = w^s = M_y^b = M_y^s = 0 \quad (42)$$

$$u_{0(x,y,t)} = \sum_{n=1}^{\infty}\sum_{m=1}^{\infty} U_{mn}\sin\ \alpha x \cos\ \beta y \quad (43)$$

$$v_{0(x,y,t)} = \sum_{n=1}^{\infty}\sum_{m=1}^{\infty} V_{mn}\cos\ \alpha x \sin\ \beta y \quad (44)$$

$$w^b_{(x,y,t)} = \sum_{n=1}^{\infty}\sum_{m=1}^{\infty} W^b_{mn}\sin\ \alpha x \sin\ \beta y \quad (45)$$

$$w^s_{(x,y,t)} = \sum_{n=1}^{\infty}\sum_{m=1}^{\infty} W^s_{mn}\sin\ \alpha x \sin\ \beta y \quad (46)$$

3. FREE VIBRATION ANALYSIS

Inserting Eqs. (37)-(40) and Eqs. (43)-(46) into Eqs. (21)-(24). The eigenvalue problem is established:

$$([K] - \omega^2[M])\{\Delta\}^T = \{0\} \quad (47)$$

$$[K] = \begin{bmatrix} K_{11} & K_{12} & K_{13} & K_{14} \\ K_{12} & K_{22} & K_{23} & K_{24} \\ K_{13} & K_{23} & K_{33} - (k_1\alpha^2 + k_2\beta^2)\Delta T & K_{34} - (k_1\alpha^2 + k_2\beta^2)\Delta T \\ K_{14} & K_{24} & K_{34} - (k_1\alpha^2 + k_2\beta^2)\Delta T & K_{44} - (k_1\alpha^2 + k_2\beta^2)\Delta T \end{bmatrix} \quad (48)$$

$$[M] = \begin{bmatrix} I_0 & 0 & -I_1\alpha & -I_3\alpha \\ 0 & I_0 & -I_1\beta & -I_3\beta \\ -I_1\alpha & -I_1\beta & I_0 + I_2(\alpha^2+\beta^2) & I_0 + I_1(\alpha^2+\beta^2) \\ -I_3\alpha & -I_3\beta & I_0 + I_4(\alpha^2+\beta^2) & I_0 + I_5(\alpha^2+\beta^2) \end{bmatrix} \quad (49)$$

$$\{\Delta\}^T = \{U_{mn}\ V_{mn}\ W^b_{mn}\ W^s_{mn}\} \quad (50)$$

where, $\alpha = m\pi/a$ and $\beta = n\pi/b$ and (U_{mn}, V_{mn}, W^b_{mn}, W^s_{mn}) are coefficients to be determined [25].

4. RESULTS

Numerical results obtained by the MATLABR2024a program based on proposing a four-variable refined plate theory, a combination of hyperbolic and polynomial shape functions employed to achieve zero transverse shear stresses on the top and bottom surfaces, without the need for a shear factor [14]. Three types of material properties are used in numerical calculations, as shown below:

Material 1:

(E_1/E_2 = open), $G_{12} = G_{13} = 0.6E_2$,$G_{23} = 0.5E_2$,$\nu_{12} = 0.25$, $E_2 = 1$ Gpa

Material 2:

($E_1/E_2 = 5$), $G_{12} = G_{13} = 0.5E_2$,$G_{23} = 0.35E_2$,$\nu_{12} = 0.3$,$E_2 = 1$ Gpa

Material 3:

(E_1/E_2 = open), $G_{12} = G_{13} = 0.6E_2$,$G_{23} = 0.5E_2$,$\nu_{12} = 0.25$,$E_2 = 6.95$ Gpa, $\alpha_2/\alpha_0 = 11.4$, $\alpha_1/\alpha_0 = 1.14$, $\alpha_0 = 10^{-6}$

Material 4:

$E_1 = 181$ Gpa, $E_2 = 10.3$ Gpa, $G_{12} = G_{13} = 7.17$ Gpa, $G_{23} = 6.21$ Gpa, $\nu_{12} = 0.28$, $\alpha_2/\alpha_0 = 22.5$, $\alpha_1/\alpha_0 = 0.02$, $\alpha_0 = 10^{-6}$

Results of nondimensional natural frequency ($\omega^*a^2*sqr(\rho/E_2h^2)$), which were computed with less mathematical complications compared to other shear theories like (higher order and third order shear deformation theories), showed good agreement. Table 1 shows the numerical values of natural frequencies evaluated using the present theory compared to other theories. Material 1 was used to provide a clear image of the effect of orthotropy ratios (E_1/E_2) on nondimensional natural frequencies for different plate laminate schemes.

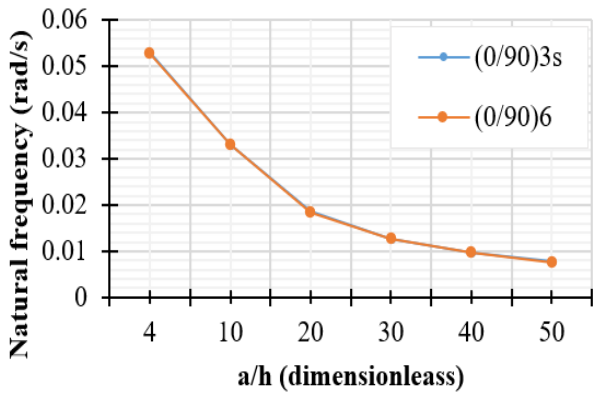

Figure 1. Natural frequency of symmetric and antisymmetric cross-ply plate using material 3 for various thicknesses and 40% of Tcr

In Table 2, the numerical values of the nondimensional natural frequency were evaluated (based on material 1) using two antisymmetric cross-ply laminated square composite plates. Values of thickness ratio (a/h) between (4-100) to show the influence of thickness on normalized fundamental frequency of laminated plates.

In Figure 1, material 3 was used to illustrates the variation of fundamental frequency (ω) with thickness ratio (a/h) range of values between (4 to 50) for a symmetric (three plies) and an antisymmetric (six plies) cross-ply laminated plate.

Table 1. Effect of orthotropic ratio on nondimensional natural frequency for two types of cross-ply simply supported square composite plate

Layup	Reference	E_1/E_2				
		3	10	20	30	40
$(0/90)_1$	Ref. [26]	6.258	6.985	7.675	8.176	8.563
	Ref. [27]	6.217	6.989	7.821	8.505	9.087
	Ref. [28]	6.149	6.916	7.692	8.311	8.826
	Ref. [29]	6.219	6.996	7.838	8.532	9.124
	Ref. [13]	6.219	6.997	7.838	8.532	9.124
	Present	6.217	6.989	7.821	8.505	9.088
$(0/90)_3$	Ref. [26]	6.610	8.414	9.840	10.696	11.273
	Ref. [27]	6.556	8.405	9.918	10.855	11.501
	Ref. [28]	6.492	8.388	9.927	10.872	11.519
	Ref. [29]	6.557	8.407	9.921	10.860	11.510
	Ref. [13]	6.557	8.407	9.921	10.860	11.510
	Present	6.556	8.405	9.918	10.855	11.501

Notes: Using material 1, thickness ratio (a/h = 5).

Table 2. Effect of thickness ratio on nondimensional natural frequency for two types of cross-ply simply supported square composite plate

Layup	Reference	a/h				
		4	10	20	50	100
$(0/90)_1$	Ref. [27]	8.355	10.568	11.105	11.275	11.300
	Ref. [28]	8.035	10.473	11.078	11.271	11.299
	Ref. [29]	8.355	10.568	11.105	11.275	11.300
	Ref. [13]	8.402	10.581	11.109	11.276	11.300
	Present	8.355	10.568	11.105	11.275	11.300
$(0/90)_3$	Ref. [27]	9.988	15.463	17.377	18.064	18.170
	Ref. [28]	9.985	15.501	17.393	18.067	18.171
	Ref. [29]	9.988	15.463	17.377	18.064	18.170
	Ref. [13]	10.004	15.463	17.377	18.064	18.17
	Present	9.988	15.463	17.377	18.064	18.17

Notes: Using material 1, Young's modulus ratio ($E_1/E_2 = 40$).

Table 3. Effect of different values of orthotropic ratio (E_1/E_2) and thickness ratio (a/h) on nondimensional natural frequency for antisymmetric angle-ply [45/-45] square composite plate

E_1/E_2	a/h	Source					
		Ref. [30]	Ref. [27]	Ref. [28]	Ref. [29]	Ref. [13]	Present
10	4	7.265	7.347	7.217	7.347	7.367	7.347
	10	8.989	8.966	8.932	8.966	8.971	8.966
	20	9.327	9.327	9.317	9.327	9.328	9.327
	50	9.438	9.438	9.436	9.438	9.438	9.438
	100	9.512	9.454	9.454	9.454	9.454	9.454
20	4	8.049	8.415	8.119	8.415	8.460	8.416
	10	10.641	10.715	10.627	10.715	10.728	10.715
	20	11.298	11.277	11.252	11.277	11.281	11.277
	50	11.507	11.455	11.451	11.455	11.456	11.455
	100	11.539	11.482	11.481	11.482	11.482	11.482
30	4	8.521	9.175	8.721	9.175	9.243	9.176
	10	11.893	12.097	11.946	12.097	12.118	12.097
	20	12.842	12.866	12.821	12.866	12.872	12.866
	50	13.157	13.115	13.108	13.115	13.116	13.115
	100	13.204	13.152	13.151	13.152	13.153	13.152
40	4	8.843	9.759	9.161	9.759	9.850	9.760
	10	12.912	13.263	13.044	13.263	13.293	13.263
	20	14.171	14.246	14.179	14.246	14.255	14.246
	50	14.601	14.572	14.561	14.572	14.574	14.572
	100	14.667	14.621	14.618	14.621	14.622	14.621

Notes: Using material 1.

By selecting material 1 for a simply supported angle-ply [45/-45] composite plate used in Table 3, nondimensional natural frequency values are evaluated for varying orthotropy and thickness values. Normalized natural frequency values demonstrated in Table 3 were calculated for thick laminated plates (thickness ratio of 4), moderately thick plates (thickness ratio of 10) and for thin plates (thickness ratio higher than 10).

Using a simply supported symmetric cross-ply $[0/90]_s$ composite plate with its length equal to its width to examine the influence of thermal loads (thermal environment) on characteristic frequency based on the present theory and literature in Table 4. The nondimensional natural frequency values (based on material 3) were evaluated at two temperature differences (0, 100°C for different thicknesses compared with

literature.

Table 4. Dimensionless natural frequency under two sets of thermal loads for equal dimensions, symmetric $[0/90]_s$ cross-play composite plate with different thicknesses

a/h	ΔT = 0°C				
	Ref. [31]	Ref. [32]	Ref. [13]	Present	Discr. %
50	18.689	18.7871	18.7382	18.7381	0.26
20	17.483	17.5231	17.9951	17.9938	2.69
10	14.702	14.7106	15.9460	15.9405	8.36
5	10.263	10.2452	11.7905	11.7711	14.89
a/h	**ΔT = 100°C**				
	Ref. [31]	Ref. [32]	Ref. [13]	Present	Discr. %
50	16.412	16.2855	14.2340	14.2338	12.60
20	17.172	17.1715	17.3242	17.3228	0.88
10	14.592	14.6369	15.7601	15.7546	7.64
5	10.226	10.2324	11.7280	11.7085	14.43

Notes: Using material 3, Young's modulus ratio ($E_1/E_2 = 40$).

Using a simply supported symmetric angle-ply $[45/-45]_2$ composite plate with its length equal to its width to examine how thermal conditions effect systems resonant frequency based on the present theory and literature in Table 5. The nondimensional natural frequency values evaluated based on two temperature differences (0, 100°C) for different thicknesses are compared with literature. Material 3 were used along with orthotropy ratio of (40).

The unforced dynamic behavior of simply supported $(45/-45)_2$ plates constructed from multiple bonded piles was analyzed under a range of thermal conditions (0%, 25%, 50%, 75%) of T_{cr}. For plates with a thickness ratio (a/h = 10) and a mass density of (1389.23 kg/m^3), the numerical data obtained from the present theory and literature are outlined in Table 6.

Figure 2 shows the correlation between thickness and natural frequency of laminated composite plate for cross-ply [0/90] and angle-ply [45/-45] composite plate under the influence of a (20%) of the plate's critical buckling temperature (based on material 3).

The effect of different design parameters, such as thickness ratio layers scheme, on the dimensionless fundamental frequency under four sets of thermal loads (20%, 40%, 60%, 80%) of Tcr for both cross-ply and angle-ply is illustrated in Table 7 (using material 3) and Table 8 (using material 4).

Table 5. Dimensionless natural frequency under two sets of thermal loads for equal dimensions $[45/-45]_2$ composite plate with different thicknesses

a/h	ΔT = 0°C			
	Ref. [31]	Ref. [13]	Present	Discr. %
50	23.225	23.2220	23.2237	0.006
20	21.812	21.7982	21.8062	0.027
10	18.333	18.3062	18.3218	0.061
5	12.544	12.5295	12.5330	0.088
a/h	**ΔT = 100°C**			
	Ref. [31]	Ref. [13]	Present	Discr. %
50	21.477	19.7677	19.7696	7.95
20	21.524	21.2478	21.256	1.245
10	18.248	18.1444	18.1601	0.482
5	12.513	12.4706	12.4741	0.311

Notes: Using material 3, Young's modulus ratio ($E_1/E_2 = 40$).

Table 6. Dimensionless natural frequency of square, symmetric $[45/-45]_2$ angle-play composite plate under variable values of thermal loads

ΔT	Ref. [13]	Ref. [31]	Ref. [33]	Present	Discr. (%)
0(Tcr)	14.262	14.312	14.438	14.268	0.307
0.25(Tcr)	12.351	12.379	12.504	12.356	0.183
0.5(Tcr)	10.085	10.082	10.209	10.089	0.068
0.75(Tcr)	7.131	7.075	7.219	7.134	0.832

Notes: 1. using material 4, thickness ratio (a/h = 10), density (ρ = 1389.23kg/m^3).
2. buckling critical temperature (T_{cr} = 7129.361°C).

Table 7. Dimensionless natural frequency under variable sets of thermal loads for equal dimensions, different piles, cross-play composite plate with different thicknesses

Layup	Tcr (°C)	a/h	Nondimensional Natural Frequency			
			20% (T_{cr})	40% (T_{cr})	60% (T_{cr})	80% (T_{cr})
(0/90)	5824.6	5	8.1294	7.0414	5.7502	4.0667
	85.639	50	10.0847	8.7336	7.1310	5.0424
$(0/90)_3$	9015.5	5	10.2872	8.9092	7.2745	5.1440
	219.7353	50	16.1573	13.9926	11.4249	8.0786
$(0/90)_9$	9376.1	5	10.5014	9.0947	7.4259	5.2510
	234.5646	50	16.6940	14.4574	11.8044	8.3470

Notes: Using material 3, Young's modulus ratio ($E_1/E_2 = 40$).

Table 8. Dimensionless natural frequency under variable sets of thermal loads for equal dimensions, different piles, and an angle-play composite plate with different thicknesses

Layup	Tcr (°C)	a/h	Nondimensional Natural Frequency			
			20% (T_{cr})	40% (T_{cr})	60% (T_{cr})	80% (T_{cr})
(45/-45)	12078.67	5	8.1486	7.058	5.7637	4.0761
	168.16	50	9.855	8.5344	6.9683	4.9273
$(45/-45)_3$	18924.5	5	10.369	8.9802	7.3325	5.185
	387.13	50	14.9551	12.9515	10.5748	7.4775
$(45/-45)_9$	19684.49	5	10.587	9.1687	7.4864	5.2938
	411.39	50	15.417	13.3514	10.9014	7.7084

Notes: Using material 4, Young's modulus ratio ($E_1/E_2 = 40$).

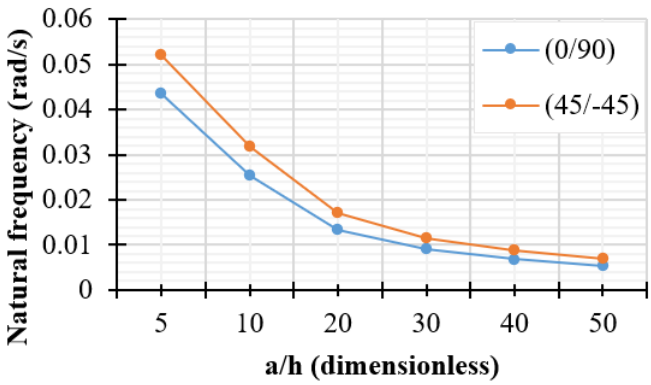

Figure 2. Natural frequency of cross-ply and angle-ply composite plates using material 3 for various thicknesses and 20% of Tcr

5. DISCUSSIONS

Table 1 results demonstrate that as (E_1/E_2) increases, nondimensional natural frequency increases due to the rise in stiffness, the main effect comes from the increase of E_1 value which directly amplifies bending stiffness via $\bar{Q}_{11}$, in addition counter effect of lowered value of E_2 allows to more shear deformation which softening the plate. As the number of layers increases, the natural frequency increases due to stiffness increase. The numerical results based on the current work showed good agreement to literature.

The present theory results demonstrated in Table 2 exhibit high convergence with other theories from literature. Also, results showed that as the thickness decreases, natural frequency decreases (the inverse values shown in Table 2 due to the effect of the (a/h) term in normalizing natural frequency), this is due to stiffness reduction which lowers natural frequency.

Numerical results in Table 3 based on the present theory shows good agreement with those of other theories. The values of the nondimensional natural frequency increase with increasing orthotropy ratio (E_1/E_2) due to Increased fiber-direction stiffness (E_1) enhances bending resistance, even when fibers are not aligned with plate axes. The transformation mechanics ensure some component of E_1 contributes to plate stiffness in all directions. Results also show that nondimensional natural frequency decrease with decreasing thickness due to reduced stiffness.

Table 4 shows a discrepancy of less than 13% for thin plates and a higher discrepancy of less than 15% for the two sets of thermal loading conditions because boundary conditions simulation differences.

Table 5 demonstrate a comparison of the present results [31], which shows a less than 8% discrepancy for thin plates and a higher discrepancy, less than 0.35%, for the two sets of thermal loading conditions. The results showed significant convergence.

The current findings illustrated in Table 6 correlate well with prior data, showing consistent, negligible variance. The effect of elevated temperature caused a decrease in the nondimensional natural frequency. In physical terms, the high-temperature environment softens the system, reducing its vibrational stiffness. This loss of rigidity increases dynamic flexibility, which can critically change the system's response to operational forces.

Results showed in Table 7 and Table 8 demonstrate that as the number of layers for cross-ply and angle-ply laminates increases, the nondimensional natural frequency increases as well for the same thickness ratio and thermal load. This is because the stiffness increases. The previous tables also demonstrate the effect of thermal load on fundamental frequency, which basically reduces nondimensional natural frequency as thermal load increases (below critical buckling temperature) for both cross-ply and angle-ply if the thickness and piles don't change, while it is greater for an angle laminated plate.as shown in Figure 2 since its stiffness is larger.

6. CONCLUSIONS

In the present paper, the four-variable refined plate theory is used for the first time to study free vibration analysis of simply supported cross-ply and angle-ply laminated composite plates under thermal loads. The displacement function, which is a combination of hyperbolic and polynomial tasks that account for zero traction stresses on free surfaces without using a shear correction factor, unlike the first-order shear deformation theory, and with less computational complexity than higher-order shear deformation theories yet maintain good agreement with all theories. The present theory reveals that the parabolic profile of transverse shear stresses is significantly modulated by ply orientation. Numerical results provide a clear image of the factors affecting the natural frequency of the plates. Basically, thermal loads significantly reduce natural frequencies by increasing the acceleration effect near the critical buckling temperature, thereby avoiding the critical temperature because buckling will occur purely due to thermal load. Also, the layer count (cross-ply or angle-ply) directly increases the plate's stiffness, altering the frequency degradation patterns. An increase in the orthotropy ratio raises the fundamental frequency due to increased stiffness. Finally, the design margin could be increased near the predicted critical buckling temperature for specific applications to provide economic efficiency. Mechanistic analysis reveals that angle-ply configurations exhibit pronounced bending-twisting coupling, which increases fundamental frequency compared to cross-ply laminates of equivalent thickness.

REFERENCES

[1] Jameel, A.N., Hussien, R.M. (2014). Vibration analysis of laminated composite plate under thermo-mechanical loading. Journal of Engineering, 20(2): 118-135. https://doi.org/10.31026/j.eng.2014.02.09

[2] Majeed, W.I., Tayeh, F.H. (2015). Stability and dynamic analysis of laminated composite plates. Journal of Engineering, 21(08): 139-159. https://doi.org/10.31026/j.eng.2015.08.09

[3] Hammed, M.B., Majeed, W.I. (2019). Free vibration analysis of laminated composite plates with general boundary elastic supports under initial thermal load. Al-Khwarizmi Engineering Journal, 15(4): 23-32. https://doi.org/10.22153/kej.2019.09.004

[4] Patro, S.S., Sutradhar, D., Behera, R.K., Sharma, N. (2018). Free vibration analysis of stiffened laminated composite plate in a thermal environment. IOP Conference Series: Materials Science and Engineering,

390: 012040. https://doi.org/10.1088/1757-899X/390/1/012040
[5] Das, S., Niyogi, A.G. (2020). Free-vibration analysis of epoxy-based cross-ply laminated composite folded plates subjected to hygro-thermal loading. Journal of The Institution of Engineers (India): Series C, 101: 541-557. https://doi.org/10.1007/s40032-020-00573-8
[6] Wu, H.L., Zhu, J., Kitipornchai, S., Wang, Q., Ke, L.L., Yang, J. (2020). Large amplitude vibration of functionally graded graphene nanocomposite annular plates in thermal environments. Composite Structures, 239: 112047. https://doi.org/10.1016/j.compstruct.2020.112047
[7] Zhai, Y.C., Su, J.M., Liang, S. (2020). Free vibration and buckling analysis of composite sandwich plates in thermal environment. Journal of Sandwich Structures & Materials, 22(8): 2604-2628. https://doi.org/10.1177/1099636218795375
[8] Daikh, A.A., Drai, A., Bensaid, I., Houari, M.S.A., Tounsi, A. (2021). On vibration of functionally graded sandwich nanoplates in the thermal environment. Journal of Sandwich Structures & Materials, 23(6): 2217-2244. https://doi.org/10.1177/1099636220909790
[9] Ibrahim, W.M., Ghani, R.A. (2017). Free vibration analysis of laminated composite plates with general elastic boundary supports. Journal of Engineering, 23(4): 100-124. https://doi.org/10.31026/j.eng.2017.04.07
[10] Hellal, H., Bourada, M., Hebali, H., Bourada, F., Tounsi, A., Bousahla, A.A., Mahmoud, S.R. (2021). Dynamic and stability analysis of functionally graded material sandwich plates in hygro-thermal environment using a simple higher shear deformation theory. Journal of Sandwich Structures & Materials, 23(3): 814-851. https://doi.org/10.1177/1099636219845841
[11] Kallannavar, V., Kattimani, S., Soudagar, M.E.M., Mujtaba, M.A., Alshahrani, S., Imran, M. (2021). Neural network-based prediction model to investigate the influence of temperature and moisture on vibration characteristics of skew laminated composite sandwich plates. Materials, 14(12): 3170. https://doi.org/10.3390/ma14123170
[12] Moradi-Dastjerdi, R., Behdinan, K. (2021). Temperature effect on free vibration response of a smart multifunctional sandwich plate. Journal of Sandwich Structures & Materials, 23(6): 2399-2421. https://doi.org/10.1177/1099636220908707
[13] Yahea, H.T., Majeed, W.I. (2021). Free vibration of laminated composite plates in thermal environment using a simple four variable plate theory. Composite Materials and Engineering, 3(3): 179-199. https://doi.org/10.12989/cme.2021.3.3.179
[14] Draiche, K., Tounsi, A. (2022). A new refined hyperbolic shear deformation theory for laminated composite spherical shells. Structural Engineering and Mechanics: An International Journal, 84(6): 707-722. https://doi.org/10.12989/sem.2022.84.6.707
[15] Sadiq, I.A., Bawa, K.H. (2018). Vibration analysis of cross-ply plates under initial stress using refined theory. Al-Khwarizmi Engineering Journal, 14(4): 34-44. https://doi.org/10.22153/kej.2018.05.002
[16] Sahu, P., Sharma, N., Dewangan, H.C., Panda, S.K. (2022). Theoretical prediction and experimental validity of thermal frequency responses of laminated advanced fiber-reinforced epoxy hybrid composite panel. International Journal of Structural Stability and Dynamics, 22(08): 2250088. https://doi.org/10.1142/S0219455422500882
[17] Saini, R., Lal, R. (2022). Axisymmetric vibrations of temperature-dependent functionally graded moderately thick circular plates with two-dimensional material and temperature distribution. Engineering with Computers, 38: 437-452. https://doi.org/10.1007/s00366-020-01056-1
[18] Azzara, R., Carrera, E., Filippi, M., Pagani, A. (2023). Vibration analysis of thermally loaded isotropic and composite beam and plate structures. Journal of Thermal Stresses, 46(5): 369-386. https://doi.org/10.1080/01495739.2023.2188399
[19] Udaiwal, A., Sharma, V.K. (2023). Investigating free vibration and buckling of laminated composites under thermal conditions. International Journal of Civil Engineering Applications Research, 4(1): 26-42. https://www.technicaljournals.org/IJCEAR/index.php/journal/article/view/5.
[20] Guo, Y.R., Guo, Y.B., Zhang, Y.X., Li, L., Zhang, D.G., Chen, S.J., Eltaher, M.A. (2024). Thermally induced vibration of a flexible plate with enhanced active constrained layer damping. Aerospace, 11(7): 504. https://doi.org/10.3390/aerospace11070504
[21] Kwak, S., Kim, H., Kim, K. (2024). Dynamic analysis of laminated composite wave plate in thermal environment using meshfree method. Journal of Vibration Engineering & Technologies, 12: 1153-1176. https://doi.org/10.1007/s42417-023-00899-4
[22] Majeed, W.I., Sadiq, I.A. (2025). Buckling analysis of composites plates using four variable refined plate theory. Revue des Composites et des Matériaux Avancés-Journal of Composite and Advanced Materials, 35(3): 567-572. https://doi.org/10.18280/rcma.350317
[23] Ebrahimi, F., Nouraei, M., Dabbagh, A. (2020). Modeling vibration behavior of embedded graphene-oxide powder-reinforced nanocomposite plates in thermal environment. Mechanics Based Design of Structures and Machines, 48(2): 217-240. https://doi.org/10.1080/15397734.2019.1660185
[24] Reddy, J.N. (2003). Mechanics of Laminated Composite Plates and Shells: Theory and Analysis. CRC Press. https://doi.org/10.1201/b12409
[25] Thai, H.T., Uy, B. (2013). Levy solution for buckling analysis of functionally graded plates based on a refined plate theory. Proceedings of the Institution of Mechanical Engineers, Part C: Journal of Mechanical Engineering Science, 227(12): 2649-2664. https://doi.org/10.1177/0954406213478526
[26] Noor, A.K. (1973). Free vibrations of multilayered composite plates. AIAA Journal, 11(7): 1038-1039. https://doi.org/10.2514/3.6868
[27] Reddy, J.N. (1984). A simple higher-order theory for laminated composite plates. Journal of Applied Mechanics, 51(4): 745-752. https://doi.org/10.1115/1.3167719
[28] Whitney, J.M., Pagano, N.J. (1970). Shear deformation in heterogeneous anisotropic plates. Journal of Applied Mechanics, 37(4): 1031-1036. https://doi.org/10.1115/1.3408654
[29] Draiche, K., Tounsi, A., Khalfi, Y. (2014). A trigonometric four variable plate theory for free vibration of rectangular composite plates with patch mass. Steel

and Composite Structures, 17(1): 69-81. http://doi.org/10.12989/scs.2014.17.1.069
[30] Swaminathan, K., Patil, S.S. (2008). Analytical solutions using a higher order refined computational model with 12 degrees of freedom for the free vibration analysis of antisymmetric angle-ply plates. Composite Structures, 82(2): 209-216. https://doi.org/10.1016/j.compstruct.2007.01.001
[31] Shen, H.S., Zheng, J.J., Huang, X.L. (2003). Dynamic response of shear deformable laminated plates under thermomechanical loading and resting on elastic foundations. Composite Structures, 60(1): 57-66. https://doi.org/10.1016/S0263-8223(02)00295-7
[32] Lal, A., Singh, B.N. (2010). Stochastic free vibration of laminated composite plates in thermal environments. Journal of Thermoplastic Composite Materials, 23(1): 57-77. https://doi.org/10.1177/0892705708103399
[33] Bhimaraddi, A., Chandrashekhara, K. (1993). Nonlinear vibrations of heated antisymmetric angle-ply laminated plates. International Journal of Solids and Structures, 30(9): 1255-1268. https://doi.org/10.1016/0020-7683(93)90015-Y

NOMENCLATURE

a,b	Plate dimensions, m
A_{ij},B_{ij},D_{ij},E_{ij},F_{ij}, H_{ij},L_{ij}	Extensional, coupling, bending, stiffnesses (N/m)
E_1,E_2,E_3	Young's modulus (GPa)
k	Number of plate layers
h	Plate thickness (m)
M^b_{xx},M^b_{yy}, M^b_{xy}	Bending moment per unit length (N m/m)
M^s_{xx}, M^s_{yy}, M^s_{xy}	Moment per unit length due to shear (N m/m)
N^T_{xx},N^T_{yy},N^T_{xy}	Thermally induced membrane forces (N/m)
Q_y, Q_x	Transverse shear force (N)
w_b,w_s	Displacement in bending, shear, respectively
x,y,z	Coordinate axes

Greek symbols

ε_{ij}	Dimensionless Strain
γ_{ij}	Dimensionless shear strain
ρ	Mass density kg/m^3
σ_{ij}(x,y,z)	Stress components (Gpa)
$\nu_{12,}$ ν_{12}	Poison's ratio

Subscripts

cr	Critical
mn	Modes of plate
1,2	Direction of fibres and transverse direction, respectively

APPENDIX

Stiffness matrix elements K_{ij} for a cross-ply laminated plate:

$$K_{11} = (A_{11}\alpha^2 + A_{66}\beta^2), K_{12} = (A_{12} + A_{66})\alpha\beta$$
$$K_{13} = -(B_{11}\alpha^3 + (B_{12} + 2B_{66})\alpha\beta^2),$$
$$K_{14} = -(E_{11}\alpha^3 + (E_{12} + 2E_{66})\alpha\beta^2)$$
$$K_{22} = (A_{66}\alpha^2 + A_{22}\beta^2),$$
$$K_{23} = -(B_{22}\beta^3 + (B_{12} + 2B_{66})\alpha^2\beta)$$
$$K_{24} = -(E_{22}\beta^3 + (E_{12} + 2E_{66})\alpha^2\beta)$$
$$K_{33} = (D_{11}\alpha^4 + 2(D_{12} + 2D_{66})\alpha^2\beta^2 + D_{22}\beta^4)$$
$$K_{34} = (F_{11}\alpha^4 + 2(F_{12} + 2F_{66})\alpha^2\beta^2 + F_{22}\beta^4)$$
$$K_{44} = (H_{11}\alpha^4 + 2(H_{12} + 2H_{66})\alpha^2\beta^2 + H_{22}\beta^4 + L_{55}\alpha^2 + L_{44}\beta^2)$$
$$A_{16} = A_{26} = B_{16} = B_{26} = D_{16} = D_{26} = E_{16} = E_{26} = F_{16} = F_{26} = H_{16} = H_{26} = L_{45} = 0$$

Stiffness matrix elements K_{ij} for an angle-ply laminated plate:

$$K_{11} = (A_{11}\alpha^2 + A_{66}\beta^2), K_{12} = (A_{12} + A_{66})\alpha\beta$$
$$K_{13} = -(3B_{16}\alpha^2\beta + B_{26}\beta^3), K_{14} = -(3A_{16}\alpha^2\beta + E_{26}\beta^3)$$
$$K_{22} = (A_{66}\alpha^2 + A_{22}\beta^2), K_{23} = -(B_{16}\alpha^3 + 3B_{26}\alpha\beta^2)$$
$$K_{24} = -(E_{16}\alpha^3 + 3E_{26}\alpha\beta^2),$$
$$K_{33} = (D_{11}\alpha^4 + 2(D_{12} + 2D_{66})\alpha^2\beta^2 + D_{22}\beta^4)$$
$$K_{34} = (F_{11}\alpha^4 + 2(F_{12} + 2F_{66})\alpha^2\beta^2 + F_{22}\beta^4)$$
$$K_{44} = (H_{11}\alpha^4 + 2(H_{12} + 2H_{66})\alpha^2\beta^2 + H_{22}\beta^4 + L_{55}\alpha^2 + L_{44}\beta^2)$$
$$A_{16} = A_{26} = B_{11} = B_{12} = B_{22} = B_{66} = D_{16} = D_{26} = E_{11} = E_{12}$$
$$= E_{22} = E_{66} = F_{16} = F_{26} = H_{16} = H_{26} = L_{45} = 0$$